Available online at www.sciencedirect.com

ScienceDirect

Ceramics International 40 (2014) 3227–3235

CERAMICS INTERNATIONAL

www.elsevier.com/locate/ceramint

Li–Y doped and codoped TiO_2 thin films: Enhancement of photocatalytic activity under visible light irradiation

Z. Hamden[a,b], D.P. Ferreira[b], L.F.Vieira Ferreira[b], S. Bouattour[a,*]

[a]*Laboratoire de Chimie Inorganique, Faculté des Sciences de Sfax, Université de Sfax, Sfax 3018, Tunisia*

[b]*Centro de Química-Física Molecular and Institute of Nanoscience and Nanotechnology, IST, Technical University of Lisbon, Lisbon, Portugal*

Received 4 August 2013; received in revised form 24 September 2013; accepted 25 September 2013
Available online 2 October 2013

Abstract

Sol – gel synthesis based on the self-assembling template method has been applied to synthesize Li–Y doped and co-doped TiO_2 not only to improve simultaneously the structural and electronic properties of TiO_2 nanomaterials but also to achieve Li–Y doping of titania with high photocatalytic reactivity. The characterization of the samples was performed by GXRD, GSDR, FT-IR, and Raman spectroscopy. According to the GXRD patterns, all the observed reflections can be indexed using the anatase form of TiO_2, Which is confirmed by ground state diffuse reflectance and micro-Raman spectra. The Li–Y doped titania materials immobilized as nanostructured thin films on glass substrates exhibit high photocatalytic efficiency for the degradation of toluidine and benzoic acid under visible light irradiation. The development of these visible light-activated nanocatalysts has the potential of providing environmentally benign routes for water treatment.

Keywords: Sol-Gel processes; Spectroscopy; TiO_2

1. Introduction

Photocatalysis has emerged as a highly promising advanced oxidation technology that can effectively address the ubiquitous demands for clean water based on the utilization of solar energy [1]. The ample verification of the effectiveness of TiO_2 to generate highly reactive hydroxyl radicals upon UV light illumination, along with its environmentally benign properties and relatively low cost, has rendered TiO_2 a key material for the complete destruction of recalcitrant organic pollutants in water resources [2] Yet, despite the marked progress in the development of TiO_2 photocatalytic materials, their practical application is challenged by two inherent limitations of TiO_2. In fact, the low quantum yield is primarily determined by the fast recombination of photogenerated charge carrier [3,4], and the wide band gap of TiO_2 semi conductor (3.2 eV for anatase) limits titania's response essentially to the ultraviolet range, which makes up a small fraction (4–5%) of the solar spectrum [5].

To overcame this issue and improve its absorption efficiency, TiO_2 is often modified, either directly or indirectly [6]. Indirect sensitization can be achieved through the use of dyes or inorganic quantum dots that absorb more efficiently the solar radiation, such as in dye-sensitized solar cells. Alternatively, TiO_2 can be more directly sensitized through the modification of its bulk or surface properties, often through the introduction of dopants, which is acommonly used method to improve photocatalytic materials.

Generally, two forms of TiO_2 in photocatalysis have been widely used including highly dispersed fine particles or suspended particles in liquid medium and thin films on supported materials [7]. When TiO_2 suspension is used in a photocatalysis system, the suspended TiO_2 needs to be separated upon the completion of each reaction cycle. This problem can be avoided by using TiO_2 applied on different types of substrates [8–10]. However, in some case TiO_2 deposited as thin films suffer from the deactivation of the photocatalytic reactivity and efficient charge recombination.

*Corresponding author. Tel.: +21 698 660 535; fax: +21 674 274 437.
E-mail address: soraa.boufi@yahoo.com (S. Bouattour).

0272-8842/$ - see front matter © 2013 Elsevier Ltd and Techna Group S.r.l. All rights reserved.
http://dx.doi.org/10.1016/j.ceramint.2013.09.114

Tada and Tanaka [11] have reported that the photocatalytic activity of TiO_2 films is smaller on a soda-lime glass substrate than onto a quartz plate. This is attributed to Na^+ ions diffused from the soda-lime glass, which act as the recombination centers or defects of the crystallinity of TiO_2.

In a previous research work, Bouattour et al. [12], studied the photocatalytic activity of prepared nanopowder of yttrium doped titania using sol–gel and solid state processes, and 2-naphthol as a pollutant model, under sunlight irradiation. Results showed a great enhancement of the photocatalytic efficiency with the incorporation of Y in samples prepared by solid grinding. Yttrium doped TiO_2 film fixed on ZSM-5 catalysts was also prepared by Okte et al. [13] using an ion exchange process. The photocatalytic results showed that yttrium incorporation enhanced the decolorization of Methyl Orange under UV irradiation.

On the other hand, Bessekhouad et al. [14] investigated the doping effect of alkaline (Li, Na, K) cations on the photocatalytic activity of TiO_2 powder under Xenon lamp irradiation. Indeed depending on the preparation technique, Li-doped TiO_2 was shown to display two contradictory behaviours. If the catalyst was prepared by sol–gel route, Li dopant reduced the performance of TiO_2, while the use of the impregnation method improved the photocatalysis of samples compared with undoped TiO_2. The effect of doping TiO_2 with Li or Rb was also studied by López et al. [15].The nanocrystalline sol–gel prepared catalysts were used for the decomposition of 2,4 dinitroaniline under UV radiation. The obtained results revealed an inhibition of the activity that was attributed to the presence of Li in the TiO_2 network which acts as an electron trap or hole trap depending on the oxidation state. So, it seems that the effect of dopants on the photocatalytic activity of doped TiO_2 depends not only on their chemical nature, but also on the preparative procedure of the materials and the pollutant structure to be degraded.

In this work, Li–Y doped or co-doped titania thin films with controlled composition were prepared using the dip coating method. The effect of the dopants on the structure and the phase stability was studied by X-ray diffraction and Raman spectroscopy. The efficiency of these samples as photocatalysts for the degradation of benzoic acid and toluidine as organic compound models, was investigated under visible light irradiation.

2. Experimental methods

2.1. Powder and film preparation

Preparation process of TiO_2 thin film elaboration is one of the major researches in photocatalysis field in order to identify an optimum condition for dip coating of TiO_2 films on various substrates. A number of methods have been employed to fabricate TiO_2 films, including sputtering, chemical vapour deposition, and sol–gel process [16,17].

In this work, polymorph titania thin films doped with 2% Li, 2%Y and 2% Li–Y was synthesized by the sol–gel process using $Ti(OBu)_4$ as precursor and pure acetic acid functioning as solvent and hydrolysis catalyst. Samples were prepared using the following materials: $YCl_3 \cdot 6H_2O$, $Ti(OBu)_4$, Li_2CO_3 (all of them from Aldrich) at the molar ratio: 0; 0.98; 0.01; 0.02; 0.98; 0, and 0.02; 0.96; 0.01 for Li doped titania, Y doped titania and Li–Y co-doped titania, respectively.

As a first step, the beads of glass were activated in a mixture of sulphuric acid and hydrogen peroxide in the proportion 60/40 in volume for 1 h, at room temperature. Then they were introduced for 2 min into the reaction vessel containing $Ti(OBu)_4$, Li_2CO_3 and/or YCl_3. Doped TiO_2 thin films are after that calcinated during 2 h at 400 °C.

The remaining solution is stirred continuously for 24 h. The final product is dried at 100 °C for 24 h and the powder is then annealed for 2 h, at 400 °C followed by a free cooling. Reference TiO_2 films and particles were always prepared following the same preparation and calcination processes but in the absence of dopants.

2.2. X-ray diffraction

The crystalline phases of Li–Y doped and co-doped TiO_2 thin films were examined by Grazing angle X-ray diffraction (GXRD) technique, using an X-ray diffractometer Panalytical Xpert with Cu $K\alpha$ radiation. The scanning range (2θ) was from 20° to 60° with a rate of 0.5°/min.

X-ray diffraction patterns of the powder samples were collected at room temperature. A Siemens/D5000 diffractometer and the Cu $K\alpha$ radiation were employed. Data were analysed in the range of $10° < 2\theta < 60°$ by step scanning, using 2θ increments of 0.02° to determine the crystallographic phases and to measure the size of the crystallites.

It is known that broadening of diffraction lines occurs for two main reasons: instrumental effects and physical origins. The latter can be roughly divided into diffraction-order independent (size) and diffraction-order-dependent (strain) broadening in reciprocal space. In this paper, the average particle size was estimated by applying the Halder–Wagner approach [18].

$$\left(\frac{\beta^*}{d^*}\right)^2 = \frac{1}{D} \times \frac{\beta^*}{(d^*)^2} + \left(\frac{\varepsilon}{2}\right)^2$$

where $\beta^* = \beta \cos\theta/\lambda$ and $d^* = 2\,\beta \sin\theta/\lambda$. Therefore, the intercept of the plot $(\beta^*/d^*)^2$ versus $\beta^*/(d^*)^2$ gives the mean value of the lattice strain ε, and the slope gives the mean apparent size D [18,19].

2.3. Ground state diffuse reflectance absorption spectra

Ground-state absorption studies were performed using all powdered samples, by means of an OLIS 14-VIS–NIR spectroscopy operating system with diffuse reflectance. The reflectance, R, from each sample was obtained by scanning the excitation monochromator from 240 to 840 nm, and the remission function, $F(R)$, was calculated using the Kubelka–Munk equation for optically thick samples (those where no further increase of the sample thickness can change the

experimentally determined R). The remission function is $F(R) = (1-R)^2/2R$ [20].

2.4. Micro-Raman set-up

Micro-Raman system was assembled in our laboratory and uses an excitation wavelength of 532 nm from a CW laser (Single mode Cobolt Samba laser, 300 mW), coupled by a 200 μm optical fibre to the spectrograph (Headwall, model 532). The Raman probe of our set-up is a Superhead 532 from H-JY. The CCD detector is from Andor, (model Newton, 1600 pixels), Peltier cooled, and works at −60 °C. 532 nm Edge, Notch and line filters are from Semrock. The system resolution is 2 cm^{-1} with a 50× Olympus long working distance objective [21].

2.5. Fourier transforms infrared spectroscopy (FTIR)

Infrared spectra were recorded with a Varian 7000 FT-IR spectrometer with a DTGS coupled detector. Samples are analysed in transmittance mode. Spectra were recorded at 1.0 cm^{-1} resolution in the 7500–400 cm^{-1} range as a ratio of 16 single-beam scans of the sample to the same number of background scans using dry air in the sample compartment. No baseline corrections are introduced. To eliminate or minimize spectral contributions from atmospheric water vapour or carbon dioxide, the instrument is purged with dry air. The original samples are diluted in KBr (about 2% w/w) and ground, with the use of an agate mortar and pestle, to form a finely divided powder. For films, an ATR accessory is used (Specac, Golden Gate MKII Diamond).

2.6. Photocatalytic activity

In each of the experiments, 50 cm^3 of approximately 5×10^{-4} mol L^{-1} solutions of the organic solute were prepared. Then, titanium dioxide films deposed on beads of glass were introduced as photocatalysts. Before irradiation, solutions were maintained in the dark for 1 h. At constant time intervals, 2 ml aliquots were sampled and then analyzed on a Cecil UV–visible spectrophotometer. The UV absorbance of the solutes was measured at their corresponding λ_{max} (which are situated between 240 and 280 nm). Calibration curves were previously established for each solute studied here. A 54 W Halogen lamp was used as visible light source. To study the effect of H_2O_2, 1.510^{-6} mol was added to the pollutant solution.

3. Results and discussion

3.1. XRD characterization

XRD is used to investigate the phase structure of the prepared samples. The grazing angle X-ray diffraction (GXRD) patterns of the Li–Y doped and co-doped TiO_2 thin films are shown in the 2θ range 20–60° (Fig. 1). All relatively sharp reflections can be indexed using the anatase tetragonal structure ($I4_1/amd$) of TiO_2 with an increase of the crystallinity

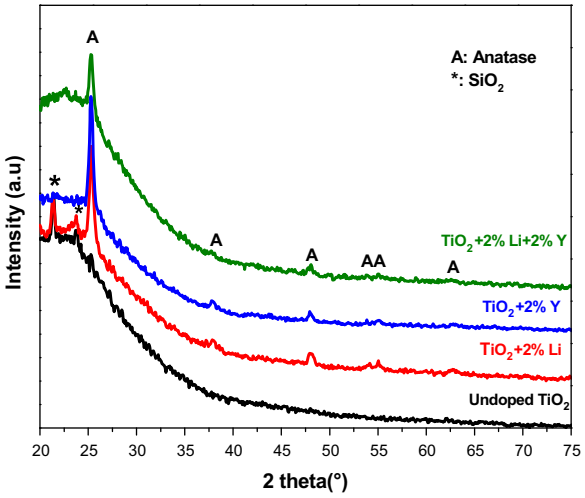

Fig. 1. XRD patterns of undoped and 2% Li–Y doped and co-doped TiO_2 thin films annealed at 400 °C.

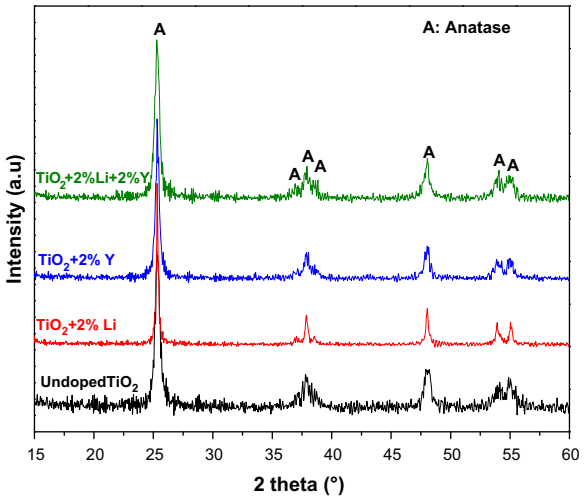

Fig. 2. Grazing angle XRD of undoped and 2% Li–Y doped and co-doped TiO_2 powders annealed at 400 °C.

of films in the presence of Li or Y dopants. No peak due to rutile or other titania phase can be detected in all samples. Additionally, diffractogrammes show a big hump recorded from $2\theta = 20°$ to 30° and two reflections associated to the SiO_2 phase, attributed to the glass substrate.

Fig. 2 shows the XRD pattern of the pure TiO_2 and Li–Y doped and co-doped TiO_2 powders. In this figure, seven distinctive TiO_2 reflections corresponding to the anatase (101, 103, 004, 112, 200, 105 and 211) crystal planes are observed. In previous work, Bouattour et al. [12] have shown that only the anatase phase is obtained for Li–Y doped and co-doped TiO_2 powder prepared by solid grinding method at 400 °C. Whereas a mixture of anatase and rutile is identified for Y or Li doped TiO_2 synthesized by the sol–gel process using a mixture of acetic and hydrochloric acids as solvent. So, one can conclude that the effect of individual dopant ions on the structure of TiO_2 is a complex problem that depends not

only on the dopant nature but also on the preparative procedure of the materials.

The average size of pure TiO_2, Li doped, Y doped and Li–Y co-doped TiO_2 nanoparticles, calcined at 400 °C, is found to be 20, 22, 12 and 14 nm, respectively, demonstrating that doping TiO_2 with Y inhibit the growth of TiO_2 particle. Ionic radius and calcination temperature are two important conditions, which strongly influence the ability of the dopant to enter into the TiO_2 crystal lattice to form stable solid solution. If the ionic radius of the doping ion is much larger, the substitution process can be suppressed [22,23]. The relatively huge difference between the Ti^{4+} (0.64 Å) radius and Y^{3+} (0.95 Å) rationalize that such substitution with Y^{3+} could not occur, Y^{3+} did not enter TiO_2 crystal lattice to substitute Ti^{4+}. Y^{3+} dopant is adsorbed at the surface of the TiO_2 particles and justifies the decreasing of anatase grain size [24] Table 1.

3.2. Ground state diffuse reflectance spectra

Ground state diffuse reflectance absorption spectra were used to probe the band structure (or molecular energy levels) in the materials since UV–vis light excitation creates photogenerated electrons and holes, (Fig. 3). The UV–vis absorption band edge is a strong function of nanoparticle titania cluster size, which can be attributed to the well-known quantum-size effect for semiconductors [25].

Table 1
Crystallite size of the Li–Y doped and co-doped samples.

Samples	Phase composition	Crystallite size (nm)
Undoped TiO_2	Anatase	20
2% Li	Anatase	22
2% Y	Anatase	12
2% (Li,Y)	Anatase	14

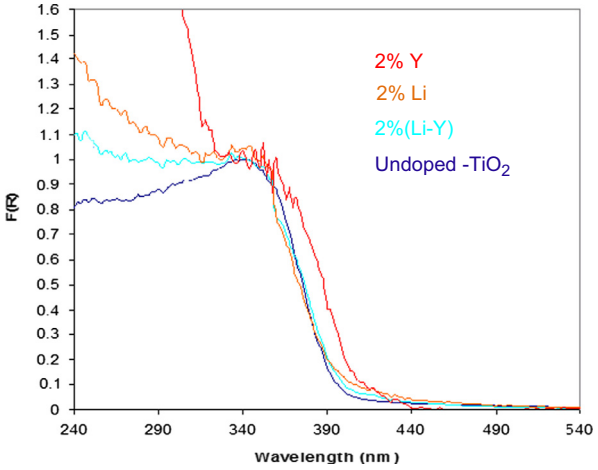

Fig. 3. Ground-state diffuse reflectance absorption spectra of undoped, Li and/or Y doped TiO_2 samples annealed at 400 °C.

The band gap of pure TiO_2 of 3.12 eV observed here is consistent with previous reports [26]. TiO_2 doped with Li, Y or Li–Y display a slightly higher absorbance than undoped oxide (Table 2). The effective optical absorption edge shifts to longer wavelength as measured by extrapolated value when the absorbance goes to zero [27]. The band gap values presented at Table 2 are slightly smaller than those observed in a previous work for similar powdered samples [12]. This is probably due to the contribution of the solvent in the hydrolysis–condensation process. In fact they employ chloride acid in addition to the acetic acid in the sol step, whereas only of the acetic acid is used in the present work.

3.3. Raman studies

The phase composition was further explored by Raman spectroscopy, where the anatase Raman modes were consistently identified for all Li–Y doped and co-doped TiO_2.

Table 2
Energy gaps, λ_{abs} (nm) of undoped, Li and/or Y doped TiO_2.

Samples	λ_{abs} (nm)	E_g (eV)
Undoped TiO_2	397	3.12
2% (Li,Y)	405	3.06
2% Li	412	3.00
2% Y	417	2.97

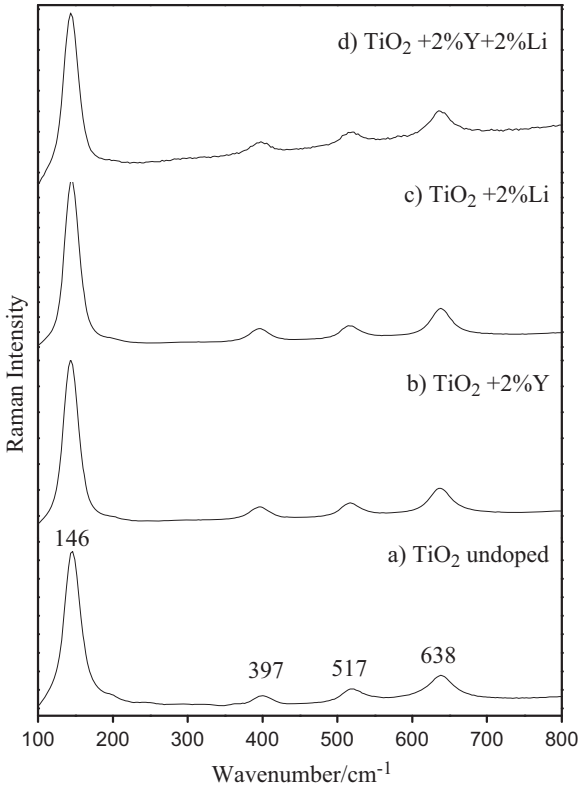

Fig. 4. Raman spectra of undoped, Li and/or Y doped TiO_2 samples annealed at 400 °C.

Table 3
Raman bands of undoped, Li and/or Y doped TiO_2.

Symmetry	Anatase (cm^{-1}) [27]	This work (cm^{-1})
Eg	148	146
B1g	397	397
A1g	516	517
Eg	638	638

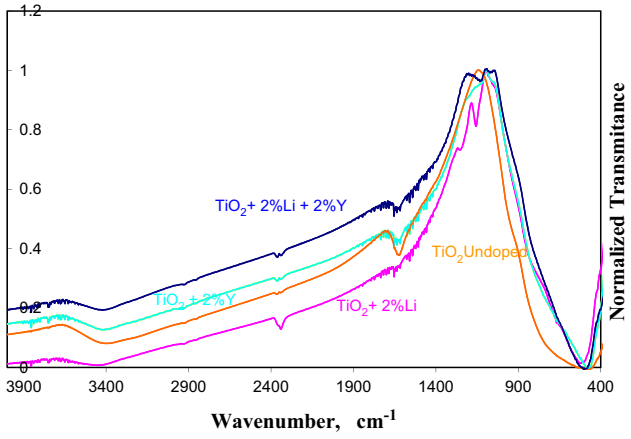

Fig. 5. FTIR studies of undoped, Li–Y doped or co-doped TiO_2 samples annealed at 400 °C.

The Raman spectrum of the sol gel TiO_2 samples is shown in Fig. 4. This spectrum exhibits the O–Ti–O peaks in the 140–700 cm^{-1} range, characteristic of anatase crystalline phase of TiO_2. A strong vibration band at 146 cm^{-1} and three larger bands at 638, 517 and 397 cm^{-1}, corresponding to Eg, B1g, A1g and Eg modes are a signature of the anatase phase [28,29]. The four samples under study present very similar Raman spectra, and no signs of Brookite, Rutile or $LiTi_2O_4$ phases were detected, only anatase phase exists in these nano-sized particles Table 3.

3.4. FT-IR studies

FTIR studies were performed in order to determine the presence of functional groups as well as to study the surface changes on the TiO_2 particles with the incorporation of dopants. Fig. 5 presents the FT-IR absorption spectra in the 400–4000 $cm-1$ region, for the Li–Y doped and co-doped TiO_2 samples, all annealed at 400 °C. All curves are normalized at the maximum transmittance to facilitate comparisons.

The presence of OH groups and water on the surface of the particles is evidenced by the appearance of a broad band about 3450 cm^{-1} accompanied by another peak around 1630 cm^{-1} for all samples. These two bands are from Ti–OH stretching modes. The titanol bands show that anatase has an important surface characteristic, i.e. may form a significatif number of hydrogen bonds which may strongly influence the adsorption and the photodegradation process. Additionally, Fig. 5 reveals that there is a decrease in the intensity of the O–H peaks in the presence of dopants and the most important effect is observed for the TiO_2 doped with Li, showing the decrease OH groups at the surface of the catalysis.

The main features to indicate in Fig. 5 are the following: these spectra reveal that in all cases TiO_2 is in the form of anatase nano-crystals [30,31]. There is a large band ~400 to 800 cm^{-1} in the undoped case that corresponds to the Ti–O–Ti stretching vibration. All doped samples exhibit a sharpening effect of this band. In the case of the two Li doped samples new peaks appear at about 1159 and 1254 cm^{-1}, similar to the ones observed for Li doped TiO_2 samples by Picquart et al. [29]. The co-doped sample exhibits a vibrational peak at 1132 cm^{-1}. The main vibration bands and peaks are shown in Table 4.

3.5. Photocatalytic degradation

To investigate the photocatalytic efficiency of the Li–Y doped and co-doped TiO_2, two aromatic organic compounds, bearing amino and carboxylic function were used as organic pollutants. In fact these two compounds belong to the families of aromatic amines and carboxylic acids respectively which are frequently found in organic dyes, fungicides, residual industrial effluent, animal repellents and defoliants. Given the serious health risks associated with the presence of these compounds in the environment, predominantly in the aqueous phase, we think that their use is interesting to study. Furthermore, if these pollutants models are degraded by the present photocatalysis, then we should expect that more complicated molecules bearing these moieties will also be prone to degradation. Although the photodegradation process using TiO_2 as catalysis, has been very effective in the decomposition and mineralization of organic pollutant in water under UV illumination, its efficacy under visible light irradiation has been only recently addressed, posing the need for development of efficient visible-light-active TiO_2 photocatalysis for pollutant abatement. In this context, the photocatalytic reactivity of Li–Y doped and co-doped TiO_2 is investigated by monitoring the time change of residual concentration ratios of aqueous solution of organic model compounds.

As shown in Fig. 6, in presence of undoped TiO_2 80% of the toluidine remained after 8 h of visible irradiation, attesting the low photocatalytic activity of the undoped TiO_2. On the other hand, a higher conversion level is observed when the photodegradation experiments are carried on using thin films, supported on beads of glasses, of Li–Y co-doped TiO_2. The conversion profile depends also on the structure of the polluant. Indeed, after 8 h exposure, the residual concentration ratio attains about 23, 35 and 19% for benzoic acid while for toluidine it reaches 47, 46 and 37% in the presence of Li, Y and Li–Y, respectively. According to the XRD results, TiO_2 exhibits the anatase structure in all the samples. This rule out the possibility that the difference in photocatalytic reactivity of the doped and co-doped thin films, is caused by the crystalline phase of TiO_2.

On the other hand a careful analysis of Fig. 6, reveals that the better photocatalytic performance is observed for benzoic

Table 4
Infrared absorption bands of undoped TiO_2, Li–Y doped and co-doped samples in the 370–4000 cm^{-1} region.

Assignment	TiO_2 (cm^{-1})	Li TiO_2 (cm^{-1})	Y TiO_2 (cm^{-1})	Li–Y TiO_2 (cm^{-1})
δ Ti–O–Ti	482	527	486	501
δ Ti–OH	3397	3458	3426	3429
δ Ti–OH	1626	1628	1624	1631

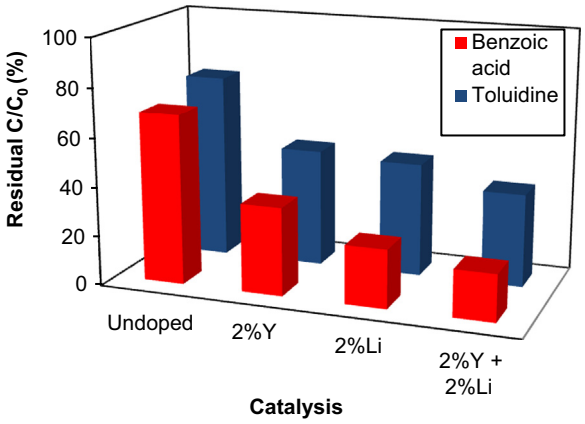

Fig. 6. Evolution of the residual concentration of the toluidine and benzoic acid vs. time after 8 h in presence of undoped and 2% Li–Y doped or co-doped TiO_2 under visible light excitation

acid in presence of TiO_2 co-doped with Li–Y since 81% of the initial concentration is degraded after 8 h. This high efficiency is probably the consequence of a high adsorption capacity of this compound toward TiO_2 surface which is the prerequisite step of the degradation process [32].

The improve in the photocatalytic efficiency observed with the introduction of dopants in this work, may be attributed to the combination of different processes: (a) the doping ions Li^+ or Y^{3+} can act as electron traps, facilitating the electron–hole separation and subsequent transfer of trapped electron to the adsorbed O_2 which acts as an electron acceptor on the surface of the TiO_2; (b) the dopants contribute to prevent the recombination of electron–hole pairs, increasing the lifetime of charge carriers, so that they can take part in photocatalytic processes; (c) decrease of the energy gap favouring higher photoexcitation efficiency under visible radiation, and giving rise to a larger population of excited species (hole–electron pairs) which is evidenced by the values listed in Table 2. On the basis of these three hypotheses, when a semiconductor oxide (TiO_2) is irradiated with light having energy higher than the band gap, a pair of a conduction band (e) and a valence band hole (h^+) is generated. The photogenerated holes at the valence band combine with adsorbed water giving mount to reactive hydroxyl radicals $OH^\bullet$. The electrons, in conduction band, join with O_2 and form $O_2^{-\bullet}$. radicals. These radicals are both strong oxidants which oxidize the organic molecules adsorbed on the surface of TiO_2 ensuing on the formation of intermediate organic species which are next completely oxidized to water and carbon dioxide.

Table 5
Apparent first-order rate constant K_{app} and correlation coefficient R^2 for photodegradation of toluidine and benzoic acid by undoped and doped TiO_2 under visible light excitation.

catalysis	Organic solute	$K_{app} \times 10^3 (h^{-1})$	R^2
TiO_2	Toluidine	8	0.98
Li–Y TiO_2		134	0.97
Li TiO_2		96	0.96
Y TiO_2		96	0.95
TiO_2	Benzoic acid	39	0.96
Li–Y TiO_2		202	0.97
Li TiO_2		195	0.95
Y TiO_2		134	0.96

3.6. Kinetic analysis

Langmuir–Hinshelwood (L–H) and first-order expressions are the most widely used expressions to explain the kinetics of heterogeneous catalytic system. It basically relates the degradation rate and reactant concentration C, in water at time t. When the adsorption is relatively weak and/or the reactant concentration is low, the system can simplified to a pseudo-first-order kinetics with an apparent first-order rate constant

$$\mathrm{Ln}(C/C_0) = -K_{app}t \quad (1)$$

where C_0 is the initial concentration.

For all catalysis, plotting $\ln(C/C_0)$ versus reaction time t yields a straight line, and the slope is the apparent rate constant. From the data reported in Table 5, the trend in the value of K_{app} is in line with the enhancement in the photocatalytic activity. The higher K_{app} value is observed for Li–Y co-doped TiO_2 followed by Li–TiO_2 and Y–TiO_2. These values corroborate with the results of Fig. 6. The higher value of K_{app} induces the better photocatalytic performance. Table 5 shows the apparent rate constants K_{app} and regression coefficients R^2 for the photodegradation of toluidine and benzoic acid.

3.7. Repeated use of the photocatalyst

The ability of a photocatalyst to be reused is one of the most important parameters which determine, from an economical point of view, the potential exploitation of a material in practical systems for water treatment. To examine the repeatability of the photocatalytic activity, the Li–Y doped and co-doped samples are used in three consecutive photodegradation cycles during 8 h of visible light irradiation. After each

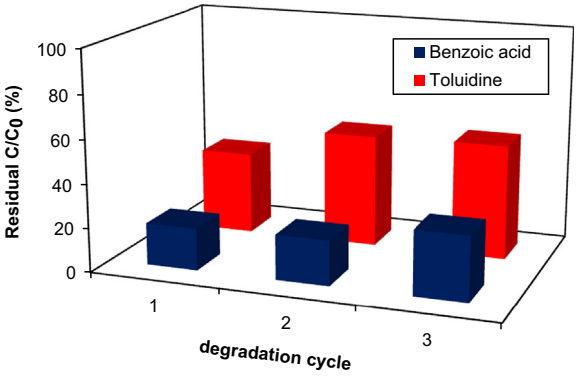

Fig. 7. Evolution of the degradation efficiency of toluidine and benzoic acid after 8 h irradiation in presence of 2% Li–Y co-doped TiO_2 photocatalysis after three degradation cycles.

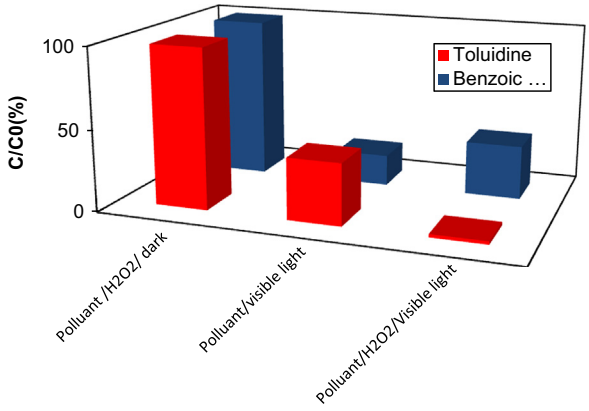

Fig. 8. Effect of H_2O_2 in the degradation of toluidine and benzoic acid after 8 h irradiation in the presence of 2% Li–Y co-doped TiO_2 photocatalysis.

decomposition cycle, the TiO_2 films supported in beads of glass were watched and used again in the same conditions.

As shown in Fig. 7 the photocatalytic efficiency decreases after three degradation cycles of the tested compounds: toluidine and benzoic acid. However, the level of decrease is not the same for the two polluants. The residual concentration attained 37, 51 and 52% and 19, 20 and 29% after three degradation cycles for toluidine and benzoic acid respectively. This result may be explained by the formation of by-products and their accumulation on the active surface sites of the photocatalyst thus making the active site on the surface less available. However, the intermediate organic species obtained during the degradation process of toluidine seems to be much more difficult to eliminate than those obtained during the degradation of benzoic acid.

3.8. Effect of H_2O_2 on the photodegradation process

Many studies have demonstrated that, under UV irradiation, H_2O_2 enhanced the TiO_2-based photocatalytic degradation of organic compounds by acting either as a source of hydroxyl radicals [33]. However, under visible light, the mechanism behind the degradation of organic compounds in the system of TiO_2/H_2O_2 is still not well-defined.

In this section, the degradation of toluidine and benzoic acid were investigated under various conditions including the processes with or without H_2O_2, and under visible light irradiation or in the dark. As shown in Fig. 8, in the dark the concentration of the two tested organic compounds do not changes even with H_2O_2 or not. However, using H_2O_2 in addition to TiO_2 co-doped with 2% Li–Y leads to the increasing of the residual concentration of benzoic acid which attained 33% after 8 h of irradiation. Whereas, the residual concentration of toluidine, decreases to 2% after 8 h of visible light excitation. Senthilkumaar et al. [34] reported that the photocatalytic efficiency of TiO_2 during the degradation process of Methylene Blue increases as the concentration of H_2O_2 increases and a further increase of H_2O_2 after optimum value leads to a decrease in the photodegradation rate. In fact, the addition of H_2O_2 increases the concentration of $OH^\bullet$ radical since it inhibit the e, h+ recombination according to Eq. (2),

$$H_2O_2 + e \rightarrow OH^- + OH^\bullet \quad (2)$$

H_2O_2 is considered to have two functions in the photocatalytic degradation. It accepts a photogenerated conduction band electron thus promotes the charge separation (Eq. (2)) and it also forms $OH^\bullet$ (Eq. (3)).

$$H_2O_2 + O_2^{-\bullet} \rightarrow OH^- + OH^\bullet + O_2 \quad (3)$$

Consequently, the degradation rate is expected to increase [35,36]. However, Wang and Hong [37] reported that further increase of H_2O_2 after a quantum level, decrease the rate of degradation. This negative effect of high concentration of H_2O_2 may be due to the formation of $OH_2^\bullet$. When the H_2O_2 concentration is high, $OH_2^\bullet$ formed is significantly less reactive than $OH^\bullet$. Thus on the catalyst surface H_2O_2 acts as a powerful $OH^\bullet$ scavenger (Eqs. (4) and (5)) along with a photogenerated holes (Eq. (6)), inhibits the generation of $OH^\bullet$ radical and thereby decreases the degradation rate.

$$H_2O_2 + OH^\bullet \rightarrow H_2O + HO_2^\bullet \quad (4)$$

$$HO_2^\bullet + OH^\bullet \rightarrow H_2O + O_2 \quad (5)$$

$$H_2O_2 + h^+ \rightarrow HO_2^\bullet + H^+ \quad (6)$$

We can conclude that for the degradation of toluidine the use of Eqs. (2) and (3) is more advantageous. A beneficial effect of H_2O_2 on the photocatalytic degradation is observed [38,39]. Whereas in the case of benzoic acid Eqs. (4)–(6) are promoted. The negative effect is evidenced by the decreasing of the degraded concentration of this acid. Similar results have been reported by Chemsedine and Bohem [40] for the degradation of chloro acid on TiO_2.

4. Conclusion

Li–Y doped and co-doped TiO_2 powders and thin films were synthesized by the sol–gel methods. (GXRD) patterns revealed that the cristallinity of films decreases for the Li–Y co-doped sample. Ground state diffuse reflectance absorption studies of

anatase samples doped with (Li,Y) reveal a shift to the visible, and the largest deviation is obtained with 2% Y. The photocatalytic activity of the prepared catalysts, under visible light irradiation, was evaluated using toluidine and benzoic acid as a pollutants model. Results showed a great enhancement in the photocatalytic efficiency with incorporation of Li–Y simultaneously. A beneficial effect of H_2O_2 on the photocatalytic degradation is observed for the toluidine degradation. Whereas in the case of benzoic acid a negative effect is evidenced by the decreasing of the degraded concentration of this acid

Acknowledgement

This work is supported by the Tunisian minister of superior education and research. Thanks are due to FCT, Portugal, for the funding projects ERA-MNT/0003/2009 and Pest-OE/CTM/LA0024/2013.

References

[1] A. Fujishima, X. Zhang, D.A. Trick, TiO_2 photocatalysis and related surface phenomena, Surface Science Reports 63 (2008) 515–582.
[2] V. Likodimos, D.D. Dionysiou, P. Falaras, CLEAN WATER: water detoxification using innovative photocatalysts, Reviews in Environmental Science and Biotechnology 9 (2010) 87–94.
[3] D. Friedmann, C. Mendive, D. Bahnemann, TiO_2 for water treatment: parameters affecting the kinetics and mechanisms of photocatalysis, Applied Catalysis B: Environmental 99 (2010) 398–406.
[4] M.A. Henderson, A surface science perspective on TiO_2 photocatalysis, Surface Science Reports 66 (2011) 185–297.
[5] A. Kubacka, M. Fernandez-García, G. Colon, Advanced nanoarchitectures for solar photocatalytic applications, Chemical Reviews 112 (2012) 1555–1614.
[6] A.V. Emeline, V.N. Kuznetsov, V.K. Rybchuk, N. Serpone, Visible-light-active titania photocatalysts: the case of N-doped TiO_2 properties and some fundamental issues, International Journal of Photoenergy (2008) 1–19.
[7] X.F. Cheng, W.H. Leng, D.P. Liu, Y.M. Xu, J.Q. Zhang, C.N. Cao, Electrochemical preparation and characterization of surface-fluorinated TiO_2 nanoporous film and its enhanced photoelectrochemical and photocatalytic properties, Journal of Physical Chemistry C 112 (2008) 8725–8734.
[8] S.Z. Chen, P.Y. Zhang, W.P. Zhu, L. Chen, S.M. Xu, Deactivation of TiO_2 photocatalytic films loaded on aluminium: XPS and AFM analyses, Applied Surface Science 252 (2006) 7532–7538.
[9] W. Dai, X. Wang, P. Liu, Y. Xu, G. Li, X. Fu, Effects of electron transfer between TiO_2 films and conducting substrates on the photocatalytic oxidation of organic pollutants, Journal of Physical Chemistry B 110 (2006) 13470–13476.
[10] J.C. Yu, W. Ho, J. Lin, H. Yip, P.K. Wong, Photocatalytic activity, antibacterial effect, and photoinduced hydrophilicity of TiO_2 films coated on a stainless steel substrate, Environmental Science and Technology 37 (2003) 2296–2301.
[11] H. Tada, M. Tanaka, Dependence of TiO_2 photocatalytic activity upon its film thickness, Langmuir 13 (1997) 360–364.
[12] S. Bouattour, A.M. Botelho do Rego, L.F. Vieira Ferreira, Photocatalytic activity of Li^+–Rb^+–Y^{3+} doped or codoped TiO_2 under sunlight Irradiation, Materials Research Bulletin 45 (2010) 818–825.
[13] A.N. Okte, O. Yilmaz, Photodecolorization of methyl orange by yttrium incorporated TiO_2 supported ZSM-5, Applied Catalysis B: Environmental 85 (2008) 92–102.
[14] Y. Bessekhouad, D. Robert, J.V. Weber, N. Chaoui, Effect of alkaline-doped TiO_2 on photocatalytic efficiency, Journal of Photochemistry and Photobiology A: Chemistry 167 (2004) 49–57.
[15] T. López, J. Hernandez-Ventura, R. Gómez, F. Tzompantzi, E. Sánchez, X. Bokhimi, A. Garcia, Photodecomposition of 2,4-dinitroaniline on Li/TiO_2 and Rb/TiO_2nanocrystallite sol–gel derived catalysts, Journal of Molecular Catalysis A: Chemical 167 (2001) 101–107.
[16] Z. Ding, X. Hu, P.L. Yue, G.Q. Lu, P.F. Greenfield, Synthesis of anatase TiO_2 supported on porous solids by chemical vapor deposition, Catalysis Today 68 (2001) 173–182.
[17] R.S. Sonawane, S.G. Hegde, M.K. Dongare, Preparation of titanium(IV) oxide thin film photocatalystby sol–gel dip coating, Materials Chemistry and Physics 77 (2002) 744–750.
[18] J.I. Langford, A rapid method for analysing the breadths of diffraction and spectral lines using the Voigt function, Journal of Applied Crystallography 11 (1978) 10–14.
[19] J.I. Langford, in: E. Prince, J.K. Stalick (Eds.), Accuracy in Powder Diffraction II', 846, NIST Spec. Pub., (Gaithersburg MA: Dept of Commerce), 1992, pp. 110–126.
[20] L.F. Vieira Ferreira, P.V. Cabral, P. Almeida, A.S. Oliveira, M.J. Reis, A.M. Botelho do Rego, Ultraviolet/visible absorption, luminescence and X-ray photoelectron spectroscopic studies of a rhodamine dye covalently bound to microcrystalline cellulose, Macromolecules 31 (1998) 3936–3944.
[21] S. Bouattour, D.P. Ferreira, A. Hamdi, L.F. Vieira Ferreira, A.M. Botelho do Rego, Spectroscopic studies of mixed pyrochlore-oxide $(Y/Gd)_2Ti_2O_7$ samples prepared via sol–gel and solid-state methodologies and calcined at different temperatures, Materials Chemistry and Physics 138 (2013) 507–513.
[22] R. Rodrigues-Talavera, S. Vargas, R. Arroyo Murillo, R. Montiel-Campos, E. Haro-Poniatowski, Modification of the phase transition temperatures in titania doped with various cations, Materials Research 12 (1997) 439–443.
[23] J. Lin, J.C. Yu, An investigation on photocatalytic activities of mixed TiO_2-rare earth oxides for the oxidation of acetone in air, Journal of Photochemistry and Photobiology A: Chemistry 116 (1998) 63–67.
[24] W. Kallel, S. Bouattour, L.F. Vieira Ferreira, A.M. Botelho do Rego, Synthesis, XPS and luminescence (investigations) of Li^+ and/or Y^{3+} doped nanosized titanium oxide, Materials Chemistry and Physics 114 (2009) 304–308.
[25] J. Zhou, Y. Zhang, X.S. Zhao, A.K. Ray, Photodegradation of benzoic acid over metal-doped TiO_2, Industrial & Engineering Chemistry Research 45 (2006) 3503–3511.
[26] R. Jaiswal, N.L. Patel, D.C. Kothari, A. Miotello, Improved visible light photocatalytic activity of TiO_2 co-doped with vanadium and nitrogen, Applied Catalysis B: Environmental 126 (2012) 47–54.
[27] A.I. Costa, L.F. Vieira Ferreira, J.V. Prata, Novel fluorescent (p-phenylene ethynylene)-calix[4];arene-based polymer: design, synthesis, and properties, Journal of Polymer Science Part A: Polymer Chemistry 46 (2008) 6477–6488.
[28] P. Falaras, A.H. Le Goff, M.C. Bernard, A. Xagas, Characterization by resonance Raman spectroscopy of sol–gel TiO_2 films sensitized by the Ru (PPh3)(2)(dcbipy)Cl-2 complex for sol, Solar Energy Materials and Solar Cells 64 (2000) 167–184.
[29] M. Picquart, L. Escobar-Alarcón, E. Torres, T. Lopez, E. Haero-Poniatowski, Structural study of lithium titanium mixed oxides prepared by sol–gel process, Materials Science 37 (2002) 3241–3249.
[30] S. Watson, D. Beydoun, J. Scott, R. Amal, Preparation of nanosized crystalline TiO_2 particles at low temperature for photocatalysis, Nanoparticle Research 6 (2004) 193–207.
[31] R.J. Tayade, P.K. Suroliya, R.G. Kulkarni, R.V. Jasra, Photocatalytic degradation of dyes and organic contaminants in water using nanocrystalline anatase and rutile TiO_2, Science and Technology of Advanced Materials 8 (2007) 455–462.
[32] U.I. Gaya, A.H. Abdullah, Heterogeneous photocatalytic degradation of organic contaminants over titanium dioxide: a review of fundamentals, progress and problems, Journal of Photochemistry and Photobiology C: Photochemistry Reviews 9 (2008) 1–12.

[33] S. Kaniou, K. Pitarakis, I. Barlagianni, I. Poulios, Photocatalytic oxidation of sulfamethazine, Chemosphere 60 (2005) 372–380.
[34] S. Senthilkumaar, K. Porkodi, R. Vidyalakshmi, Photodegradation of a textile dye catalyzed by sol–gel derived nanocrystalline TiO_2 via ultrasonic irradiation, Journal of Photochemistry and Photobiology A: Chemistry 170 (2005) 225–232.
[35] C. Hachem, F. Bocquillon, O. Zahraa, M. Bouchy, Decolourization of textile industry wastewater by the photocatalytic degradation process, Dyes and Pigments 49 (2001) 117–125.
[36] P. Salvador, F. Decker, The generation of hydrogen peroxide during water photoelectrolysis at n-titanium dioxide, Journal of Physical Chemistry B 88 (1984) 6116–6120.
[37] Y. Wang, C.S. Hong, Effect of hydrogen perox ide, periodate and persulfate on photocatalysis of 2-chlorobiphenyl in aqueous TiO_2 suspensions, Water Research 33 (1999) 2031–2036.
[38] Z. Mengyne, C. Shifu, T. Yaowu, Photocatalytic degradation of organophosphorus pesticides using thin films of TiO_2, Journal of Chemical Technology and Biotechnology 64 (1995) 339–344.
[39] K. Tanaka, T. Hisanaga, K. Harada, Efficient photocatalytic degradation of chloral hydrate in aqueous semiconductor suspension, Journal of Photochemistry and Photobiology A: Chemistry 48 (1989) 155–159.
[40] A. Chemsedine, H.P. Bohem, A study of the primary step in the photochemical degradation of acetic acid and chloroacetic acids on a TiO_2 photocatalyst, Journal of Molecular Catalysis 60 (1990) 295–311.